

Intermolecular Interactions in the Solid State of Ionic Secondary Mannich Bases

Jerzy Kołodziejczak,^{*,†} Agnieszka Adamczyk-Woźniak,[‡] Barbara Hachuła,[§] Maciej Barys,[†] Henryk T. Flakus,[§] Andrzej Sporyński,[‡] and Aleksander Koll^{*,†}

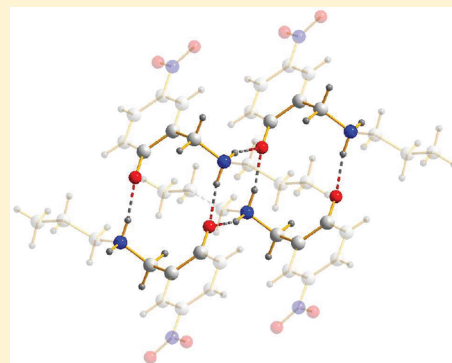
[†]Faculty of Chemistry, Wrocław University, F. Joliot-Curie 14, 50-383 Wrocław, Poland

[‡]Faculty of Chemistry, Warsaw University of Technology, Noakowskiego 3, 00-664 Warsaw, Poland

[§]Institute of Chemistry, University of Silesia, Szkolna 9, 40-006 Katowice, Poland

S Supporting Information

ABSTRACT: Two new secondary Mannich bases, 4-bromo-2-[(aminopropyl)methyl]-phenol (**1**) and 4-nitro-2-[(aminopropyl)methyl]-phenol (**2**), were synthesized. Crystal structures were determined at liquid nitrogen temperature. It was found that in both compounds the proton transfer forms exist in the solid state. In the case of **1**, this was unexpected, because of the weak acidity of *p*-bromophenol being the parent component of this Mannich base. The reason for that was found to be the formation of the O[−]⋯H–N⁺ hydrogen bonded tetramer in the solid state. Two cyclic aggregates R₄²(8) and R₂²(12) describe the pattern of hydrogen bonded interactions in the crystals of both compounds. Additionally, C–H⋯π interactions stabilize the crystal structures. The hydrogen bonds in **1** are slightly stronger (N⋯O distances 2.708 and 2.733 Å) than in **2** (2.721 and 2.765 Å, respectively) despite the fact that *p*-nitrophenol participating in **2** is a stronger acid. The influence of permittivity of surroundings and the hydrogen bonding pattern on the properties of intermolecular hydrogen bonds are discussed on the basis of B3LYP and MP2 calculations with basis sets 6-31+G(d,p) and 6-31++G(2d,2p). The coupling between hydrogen bonds in crystals was studied with the application of the IR spectra of isotopically diluted species. It was found that such a coupling is stronger for **2**, forming weaker hydrogen bonds. Both the theory of IR spectra and quantum chemical calculations demonstrate that the source of the observed behavior is electronic participation in vibronic absorption.



INTRODUCTION

2-(*N,N*-Dialkylaminomethyl) phenols (Mannich bases) are able to form intramolecular hydrogen bonds, not perturbed by the π electronic coupling between acid and base centers. The considered interactions appeared to be a very useful model in the study of the nature of the hydrogen bond.^{1,2} The specific advantage of using such a model system is the thermodynamic and structural stability of the intramolecular hydrogen bond. Because of different entropy contributions in breaking such hydrogen bonds in comparison with intermolecular analogues, such systems are stable in a wide range of solvent polarities and temperatures.³ The model allowed, for example, the study of conditions of proton transfer avoiding complicated association of complexes and partners of the interaction.⁴

Nevertheless, in the case of proton transferred forms in nonpolar and low polar solvents, dimeric, nonpolar aggregates with symmetry centers were suggested,⁵ which were documented in the solid state.^{1,6}

Recently, computational studies were devoted to investigations of the bridged proton dynamics in the intramolecular O–H⋯N bridge of tertiary Mannich bases.^{7–10} The influence of the environment was investigated by comparison of the molecular properties of these systems in the gas-phase and solid

state⁸ as well as in solution.⁹ Extension of such studies on possible aggregation of the forms with intermolecular hydrogen bonds was possible due to the synthesis of the “secondary” Mannich bases with CH₂–N(H)–alkyl moiety in works of Bujnowski et al.^{11,12} Secondary Mannich bases form simultaneously intramolecular and intermolecular hydrogen bonds. Competition of these two interactions was recently studied.¹³ Crystal structure determination, spectroscopic studies in solvents of different polarities, and theoretical calculations were performed. The linear chains of intermolecular N–H⋯O hydrogen bonds were found in the solid state, while intramolecular OH⋯N hydrogen bonds also remained. It was shown that formation of the intermolecular hydrogen bonds led to substantial strengthening of the intramolecular interactions. Density functional theory (DFT) calculation on monomers and cyclic and linear aggregates supported this observation. It was found that attack of either acid or base molecules on secondary Mannich bases was effective in strengthening the intramolecular hydrogen bonds. Such effects were not possible

Received: February 15, 2011

Revised: December 20, 2011

Published: January 4, 2012

to be observed in the previously studied tertiary Mannich bases. In the work presented here, we broaden the studies on interaction between secondary Mannich bases in the solid state, when the zwitterionic species are formed, on the example of two compounds: 4-bromo-2-[(aminopropyl)methyl]-phenol (**1**) and 4-nitro-2-[(aminopropyl)methyl]-phenol (**2**). These compounds, differing only by substituents at the para-position in the phenyl ring were synthesized, their crystal structures were determined, and careful IR studies in polarized light of isotopically neat as well as deuterated species at room and liquid nitrogen temperatures were performed. Experimental data and quantum chemical calculations demonstrate considerable influence of substituents on molecular interactions in the solid state.

It was found that intramolecular hydrogen bonds in **1** and **2** are completely broken. The NH_2^+ groups are double proton donors to different PhO^- groups in neighboring molecules forming cyclic tetramers, which is probably the main factor stabilizing the proton transfer (PT) forms of these molecules. A similar pattern of hydrogen bonds was described previously in the crystal of an intermolecular complex between 2,4-dinitrophenol and morpholine.¹⁴

The pattern of hydrogen bonded net in both crystals can be described as $\text{R}_2^2(12)$ and differently oriented $\text{R}_4^2(8)$ units^{15,16} in basic tetramers. Additionally, the stability of the crystal is enhanced due to weak $\text{C}-\text{H}\cdots\pi$ and $\text{C}-\text{H}\cdots\text{O}$ interactions. Stacking contacts between aromatic rings were not found.

In the case of previously studied tertiary *para*- NO_2 Mannich bases, the zwitterionic forms were observed,¹⁷ but for *para*-Br similarly to *para*-Cl derivatives the acidity of phenols was too low to form the zwitterionic structures in the solid state.¹

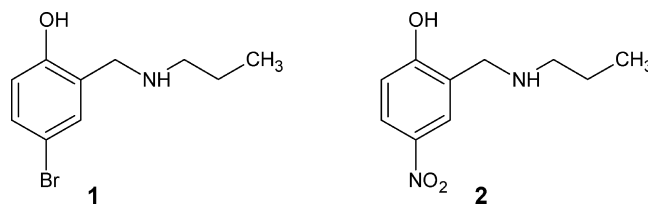
In extension of our previous study, it was interesting to learn to what extent the interaction between particular hydrogen bonds takes place. A very efficient method to study such tasks was developed by Flakus et al.^{18–22} They have revealed that dynamic coupling in hydrogen bond systems, involving proton (or deuteron) stretching vibrations in the hydrogen bonds, and the electronic motions in the associated molecules stabilize crystal lattices. In such circumstances, a nonrandom distribution of proton and deuterons takes place for the vast majority of hydrogen bonded crystalline systems. The consequence of these results in the IR spectra attributed to the “residual” hydrogen bonds in not entirely deuterated crystals, which remain unchanged, despite the growing concentration of deuterons in their lattices (the H/D isotopic “self-organization” effects). Identical hydrogen isotope atoms, proton or deuterons, are grouped together in fragments of a lattice (domains). A particular way of occurring of the H/D isotopic “self-organization” for an individual crystal depends on the electronic properties of the associating molecules. Study of the IR crystalline spectra, measured in polarized light, gives the possibility to identify the hydrogen bonds which are active in these interactions. Quantum mechanical calculations were performed to explain the differences in coupling in crystals **1** and **2**, as well as the influence of surrounding polarity.

EXPERIMENTAL SECTION

Synthesis and Purification. Synthesis of compounds **1** and **2** was performed by the amination–reduction of the corresponding aldehyde and *n*-propylamine. Analytical samples and single crystals for X-ray measurements have been obtained by crystallization from hexane.

Synthesis of 4-Bromo-2-[(aminopropyl)methyl]-phenol (1**).** Solution of 3-bromo-6-hydroxybenzaldehyde (2.50 g, 0.0123 mol) in

Chart 1. The Investigated Compounds



methanol (15 mL) was prepared at room temperature and stirred. On addition of *n*-propylamine (0.82 g, 0.0138 mol, 1.14 mL) heating evolved and the reaction mixture became intensely yellow. Stirring was continued overnight. Then NaBH_4 (0.18 g, 0.0047 mol) was added portion-wise resulting in the discoloration of the solution. TLC of the mixture ($\text{CHCl}_3:\text{CH}_3\text{OH}$, 95:5, v/v) revealed no traces of the starting material or the corresponding Schiff base. The desired product separated as a white powder after evaporation of about one-third of the volume of the mixture. The solid was filtered off and dried in air.

4-Bromo-2-[(aminopropyl)methyl]-phenol (1.48 g, 56%), mp 93–95 °C (from hexane). Found: C, 49.1; H, 5.7; N, 5.7. Calc. for $\text{C}_{10}\text{H}_{14}\text{BrNO}$: C, 49.2; H, 5.7; N, 5.7. δH (400 MHz; CDCl_3) 0.94 (3H, t, $J_{1,2}$ 7, Me), 1.55 (2H, m, CH_2), 2.62 (2H, t, $J_{1,2}$ 7, CH_2), 3.95 (2H, s, Ar- CH_2 -N), 6.70 (1H, d, $J_{1,2}$ 8, Ar), 7.09 (1H, m, Ar), 7.22–7.25 (1H, m, Ar). δC (100 MHz; CDCl_3) 11.5, 22.6, 50.3, 52.1, 110.5, 118.1, 124.5, 130.6, 131.2, 157.6.

Synthesis of 4-Nitro-2-[(aminopropyl)methyl]-phenol (2**).** Suspension of 3-nitro-6-hydroxybenzaldehyde (2.50 g, 0.015 mol) in methanol (30 mL) was prepared at room temperature and stirred. On addition of *n*-propylamine (0.89 g, 0.015 mol, 1.23 mL) additional portion of the solid separated and another 20 mL of methanol was added. Stirring of the suspension was continued for 5 h at room temperature, and then about half of the volume of the mixture was evaporated under reduced pressure. Yellow solid of the Schiff base contaminated with traces of the starting aldehyde was filtered off and was purified by crystallization from hexane (2 g, 49% yield). The Schiff base (1.5 g, 0.0071 mol) was dissolved in MeOH, and NaBH_4 (0.12 g, 0.0032 mol) was added portion-wise, with intense stirring resulting in a yellowish suspension. The desired product separated as a white powder after evaporation of about half of the mixture's volume. The solid was filtered off and dried in air.

4-Nitro-2-[(aminopropyl)methyl]-phenol (1.0 g, 66%), mp 190–192 °C (from hexane). Found: C, 57.1; H, 6.6; N, 13.2. Calc. for $\text{C}_{10}\text{H}_{14}\text{N}_2\text{O}_3$: C, 57.1; H, 6.6; N, 13.3. δH (400 MHz; CDCl_3) 0.95 (3H, t, $J_{1,2}$ 7.2, Me), 1.55–1.64 (2H, m, CH_2), 2.66 (2H, t, $J_{1,2}$ 7.2, CH_2), 4.09 (2H, s, Ar- CH_2 -N), 6.84 (1H, d, $J_{1,2}$ 9, Ar), 7.95 (1H, m, Ar), 8.09 (1H, m, Ar). δC (100 MHz; CDCl_3) 11.5, 22.3, 50.4, 52.0, 116.7, 122.1, 124.3, 125.1, 139.9, 165.2.

Crystal Structure Determination. Crystal structure was evaluated at the Crystallographic Laboratory of the Faculty of Chemistry of Wrocław University. CCDC-804823 for **1** and CCDC-804824 for **2** contain the supplementary crystallographic data for this paper. This data can be obtained free of charge via www.ccdc.cam.ac.uk/conts/retrieving.html (or from the Cambridge Crystallographic Data Centre, 12 Union Road, Cambridge CB2 1EZ, UK; fax: (+44)1123-336-033; e-mail: deposit@ccdc.cam.ac.uk).

Crystal Data of **1.** $\text{C}_{10}\text{H}_{13}\text{BrNO}$, $M = 243.12$, monoclinic, $a = 10.935(2)$, $b = 5.6281(3)$, $c = 16.630(3)$ Å, $\alpha = \beta = 102.98(2)^\circ$, $U = 997.4(3)$ Å³, $T = 100(2)$ K, space group $P2_1/c$ (No. 14), $Z = 4$, 11696 reflections measured, 2304 unique ($R_{\text{int}} = 0.0285$) which were used in all calculations. The final $wR(F^2)$ was 0.0458 (all data).

Crystal Data of **2.** $\text{C}_{10}\text{H}_{14}\text{N}_2\text{O}_3$, $M = 210.23$, triclinic, $a = 5.391(3)$, $b = 9.633(3)$, $c = 10.258(3)$ Å, $\alpha = 73.51(3)$, $\beta = 87.74(3)$, $\gamma = 82.89(3)^\circ$, $U = 506.9(3)$ Å³, $T = 100(2)$ K, space group $P\bar{1}$ (No. 2), $Z = 2$, 3401 reflections measured, 1752 unique ($R_{\text{int}} = 0.0117$) which were used in all calculations. The final $wR(F^2)$ was 0.0955 (all data).

The structures of **1** and **2** were solved and refined using SHELXS-97 and SHELXL-97 software.²³

Additional data related to crystal measurements can be found in Table S1 of Supporting Information.

IR Spectra. FTIR spectra were determined in KBr pellets (3 mg in 200 mg KBr), as well as in the crystal form of “normal” and deuterated species at room temperature and at liquid nitrogen temperature. IR spectra of crystals were measured on an FTIR MAGNA 560 spectrophotometer (Nicolet) with a resolution of 2 cm^{-1} , using polarized IR radiation. 10-fold repetition was applied. Crystals for spectral studies were obtained by crystallization from the melt, between two closely spaced CaF_2 windows. This way, sufficiently thin crystals could be obtained. The absorbance of the $\nu(\text{OH})$ band in the IR spectra was about 0.5. From the crystalline mosaic, suitable monocrystalline fragments were selected and then oriented with the help of a polarization microscope.

These crystals were exposed to the experiment by use of a thin diaphragm with a 1.5 mm diameter hole. In each measurement, two different, mutually perpendicular orientations of the electric field vector “E” were applied, with respect to the crystalline lattice. Spectra were recorded in a similar manner for the deuterium derivatives. Deuterated species were obtained by 4-fold crystallization from D_2O .

Quantum Mechanical Calculations. The calculations were performed with the help of Gaussian 09 programs.²⁴ The DFT B3LYP/6-31+G(d,p) method was used. All frequencies in harmonic approximation for states with minimum of energy were positive. Some calculations with extended 6-311++G(2d,2p) basis set at B3LYP and MP2 levels were performed, to check which level of theory is sufficient to reproduce the experimentally determined values. In order to model ionic forms dependence on surroundings polarity, the PCM model with various solvents was applied.

Electric Permittivity. Electric permittivity has been measured in the frequency range of 1 kHz–1 MHz using Hewlett-Packard 4284A LZC equipment as described by Szulia and co-workers.²⁵ The precision of the measurements was 2% for electric permittivity. Such precision could be reached by means of calibration of measuring systems using at least two standard samples of well-known permittivity. Samples were made as pellets of 10 mm in diameter and about 1–2 mm thick. Electrodes were cut from commercially available copper-foil with silver nanoparticles immersed in a thin layer of glue and affixed to the prepared pellets.

RESULTS AND DISCUSSION

Crystal Structure Description. The crystal structure of **1** contains only one symmetry independent molecule (Figure 1).

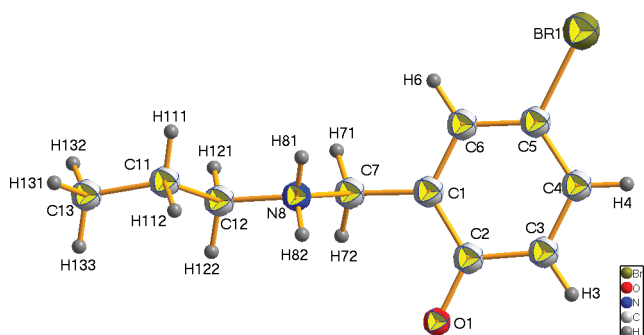


Figure 1. Molecular structure of **1**, according to the crystal structure determination. Thermal vibrations of non-hydrogen atoms are drawn at 50% of probability.

Some selected structural parameters of this molecule are presented in Table S2, Supporting Information. The molecule in the crystal exists in the zwitterionic form, where the proton was transferred from an O–H group to nitrogen atom. Also the length of C–O bond is characteristic for the ionic form of the phenolic part of a molecule. Two slightly different $\text{O}^-\cdots\text{H}-\text{N}^+$ hydrogen bonds are responsible for organization of the

molecules in the crystal (cf. Figures S1 and S2 in Supporting Information). The pattern of organization of molecules being in direct contact can be described according to the system of Etter and Bernstein^{15,16} as $\text{R}_2^2(12)$ and $\text{R}_4^2(8)$ (Figure 2). Each of

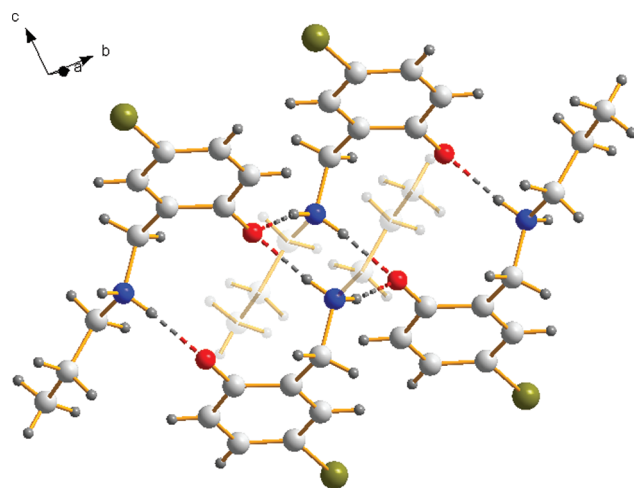


Figure 2. Basic pattern of organization of the net of hydrogen bonds in the crystal of **1**, view along axis *a*.

these cyclic forms is made of two types of hydrogen bonds described in Table S3, Supporting Information. The angle between $\text{R}_2^2(12)$ and $\text{R}_4^2(8)$ planes, built of N and O atoms, was found to be $50.6(3)^\circ$. No intramolecular hydrogen bonds or stacking of aromatic rings were detected. Stability of the crystal was enhanced by C–H $\cdots\pi$ interactions (Table S4, Supporting Information), as it is demonstrated in Figure 3.

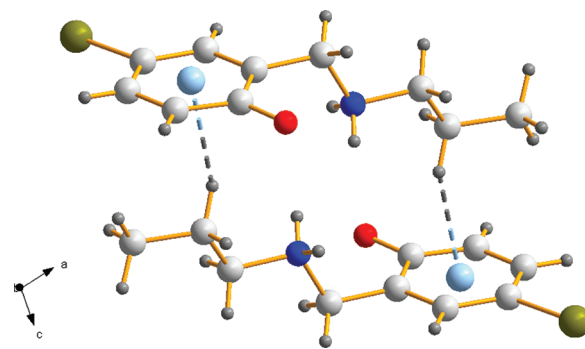


Figure 3. Weak interactions in the crystal of **1**. View along the *b* axis.

Selected structural parameters of **2** are presented in Table S5, Supporting Information. Crystal structure of **2** is arranged, similar to **1**, by the net of intermolecular $\text{O}^-\cdots\text{H}-\text{N}^+$ hydrogen bonds (Table S6, Supporting Information) and weaker interactions of C–H $\cdots\pi$ (Table S7, Supporting Information) character as well by C–H $\cdots\text{O}$ hydrogen bonds to oxygen atoms of the $-\text{NO}_2$ groups. The structure analysis shows that, as in **1**, there exist neither intramolecular hydrogen bonds, nor stacking of aromatic rings. In the crystal **2** only one independent molecule exists, whose structure is demonstrated in Figure 4, while the intermolecular hydrogen bonding network is depicted in Figure 5. Geometric parameters of this molecule are presented in Table S5, Supporting Information. The net of weak CH $\cdots\pi$ (Table S7, Supporting Information) and C–H $\cdots\text{O}$ interactions is presented in Figure 6.

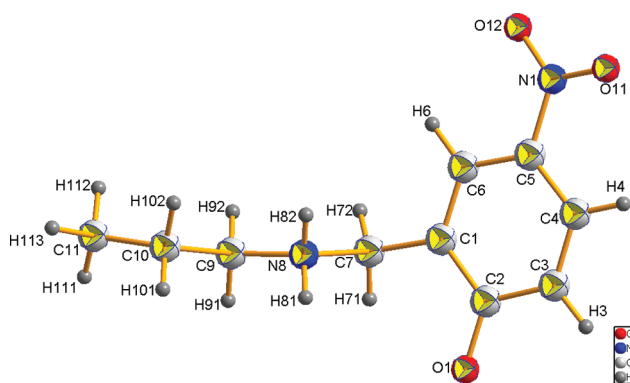


Figure 4. Molecular structure of **2**. Thermal vibrations of non-hydrogen atoms are drawn at 50% of probability.

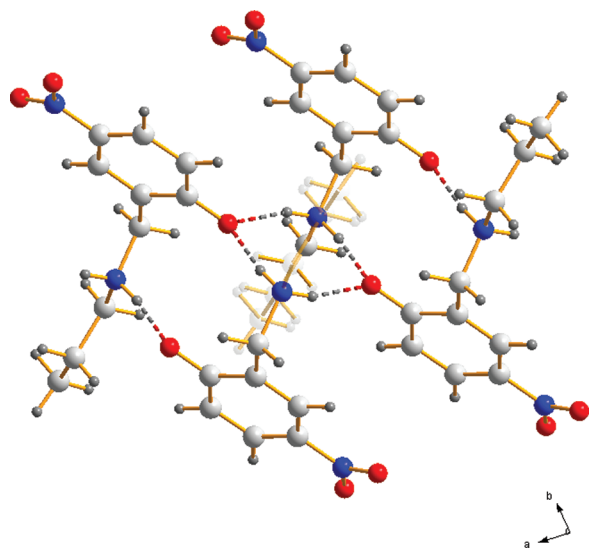


Figure 5. Pattern of hydrogen bonds net in the crystal of **2**. View of tetramer along the crystal axis *c*. The angle between R(8) and R(12) planes is equal to 62.3(3)°.

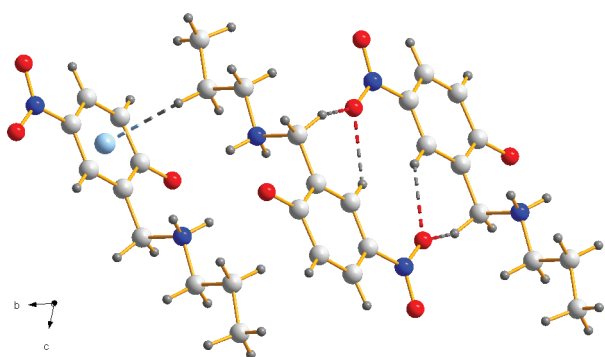


Figure 6. The pattern of C–H... π and C–H...O interactions in the crystal of **2**, view along axis *a*.

Calculations. In order to understand the nature of the differences in the molecular interactions, detailed inspection of the geometry of molecules **1** and **2** by theoretical methods has been performed. Monomeric units (cf. Figures 1 and 4, Tables S2 and S5, Supporting Information) were selected from tetramers presented in the crystal structures of **1** and **2** (Figures 2 and 5). Inspection of the pattern of ring bond lengths shows some asymmetry with respect to the 2–5 axis.

Such a property could be characteristic for intramolecular hydrogen bonds,²⁶ but in the investigated case, the intramolecular hydrogen bonds do not exist. Performing calculations in the gas phase, one can expect avoiding consequences resulting from the crystal packing forces. We have used a few variants of calculations seeking the best reproduction of the geometry of molecules in the crystals. The results are presented in Table 1.

The last rows for each molecule in Table 1 present the estimation of the variance of ring bond lengths. Increase of this parameter points out the stronger electronic coupling between substituents in the ring. Appearance of ionic forms of hydrogen bonds leads to a significant increase of this parameter (4–5-fold in our case). The standard calculations in the gas phase (variants A, Table 1) resulted in bad reproduction of the ionic structure of the crystals as the minimum of energy is for the O–H...N type of intramolecular hydrogen bond.

Columns B and C present the two different structures (I and II) obtained in the calculations of basic tetramers existing in both crystals (Figures 2 and 5). To obtain deeper minima for the proton transfer forms, the calculations were performed in PCM variant, for water as a solvent. It was successful — the most characteristic is shortening of C–O distance as it is natural for phenolates. These distances are shorter, as a rule, in **2** than in **1**.

In order not to discuss all distances separately, the values of square roots of mean squared deviations of calculated bond lengths between heavy atoms and related experimental ones, as well as ring bond lengths variation for each molecule, are analyzed. The largest “average deviations” have been found for molecular structure A with a nonionic intramolecular hydrogen bond. Structures I and II, obtained in optimization of tetramers, reveal much better reproduction of the geometry found in the crystals. Interestingly, results of variant D are similar to variant A for **1**; calculations for the monomer of **1**, at the level of B3LYP/6-31+G(d,p) in water as a solvent, still gives the molecular form of the Mannich base. It accords with our supposition that for a Mannich base built of *p*-bromophenol with low acidity ($pK_a = 9.37$)²⁷ the necessary condition to obtain minimum for O[−]...H–N⁺ hydrogen bond is to construct a tetramer of zwitterionic forms.

In the case of **2** ($pK_a = 7.15$), this condition seems not to be essential — one obtains the minimum for zwitterionic form of monomer, similarly as for molecules optimized as tetramers.

In molecule **2** three ionic structures (B, C, and D) show similar standard deviations, and obviously better reproduce crystal structure than molecular structure A, obtained in the gas phase. In variants E, F, and G, selected monomers were calculated at B3LYP/6-31++G(2d,2p), MP2/6-31+G(d,p), and MP2/6-31++G(2d,2p) levels, respectively. In both molecules, the zwitterionic structures were obtained. The standard deviations were the lowest, which means the best reproduction of the experimental geometry. It appears that higher basis sets of DFT calculation and MP2 calculations give sufficient conditions to obtain zwitterionic forms of hydrogen bonds in both molecules in a polar solvent.

All ionic structures in variants B, C, D, E, F, and G for *para*-nitro compound give high values of the variance of bond lengths. It is worthwhile to compare these variances in molecules **1** and **2**. Table 1 clearly shows that in **2** the variance in all cases of calculations is at least two times higher than in **1**. It points out the higher electronic coupling between substituents in molecule **2**. This explains why there is coupling between hydrogen bonds in **2**, demonstrated in IR experiments

Table 1. Reproduction the Basic Structural Parameters of Molecules 1 and 2 in the Crystal^a

compound	experimental	calculated structures ^b						
		A	B	C	D	E	F	G
1								
Br1–C5	1.910(2)	1.9105	1.9207	1.9196	1.9169	1.9321	1.9089	1.9065
O1–C2	1.315(2)	1.3592	1.3090	1.3118	1.3610	1.3095	1.3307	1.3213
N8–C12	1.496(2)	1.4695	1.5034	1.4967	1.4732	1.4893	1.4846	1.4809
N8–C7	1.503(2)	1.4751	1.5140	1.5130	1.4766	1.5024	1.4947	1.4929
C1–C6	1.398(2)	1.3988	1.3994	1.4022	1.3983	1.3906	1.3982	1.3955
C1–C2	1.423(2)	1.4128	1.4330	1.4338	1.4139	1.4299	1.4283	1.4268
C1–C7	1.503(2)	1.5135	1.5013	1.5036	1.5152	1.5054	1.5013	1.5007
C2–C3	1.416(2)	1.3998	1.4248	1.4250	1.4003	1.4159	1.4156	1.4144
C6–C5	1.386(2)	1.3928	1.3915	1.3901	1.3938	1.3874	1.3943	1.3908
C5–C4	1.389(2)	1.3944	1.3960	1.3959	1.3938	1.3897	1.3983	1.3942
C3–C4	1.382(2)	1.3937	1.3906	1.3901	1.3953	1.3874	1.3958	1.3935
C11–C12	1.521(2)	1.5295	1.5255	1.5280	1.5291	1.5233	1.5194	1.5180
C11–C13	1.526(2)	1.5328	1.5334	1.5333	1.5328	1.5293	1.5259	1.5257
Sq MSD ^c		0.018	0.008	0.007	0.018	0.007	0.008	0.007
A ^d	237	47	278	293	49	277	158	178
2								
N1–C5	1.440(3)	1.4591	1.4206	1.4232	1.4190	1.4192	1.4376	1.4385
O1–C2	1.297(2)	1.3478	1.2822	1.2872	1.2854	1.2790	1.3045	1.2976
N8–C9	1.494(2)	1.4715	1.5058	1.5021	1.4991	1.4956	1.4904	1.4858
N8–C7	1.497(2)	1.4760	1.5153	1.5164	1.5093	1.5066	1.4991	1.4959
C1–C6	1.382(3)	1.3914	1.3821	1.3856	1.3793	1.3730	1.3883	1.3854
C1–C2	1.421(3)	1.4194	1.4480	1.4494	1.4517	1.4471	1.4395	1.4371
C1–C7	1.500(2)	1.5145	1.5008	1.5039	1.5065	1.5030	1.4994	1.4989
C2–C3	1.427(2)	1.4053	1.4382	1.4386	1.4366	1.4322	1.4271	1.4247
C6–C5	1.394(3)	1.3972	1.4118	1.4103	1.4099	1.4036	1.3997	1.3954
C1–C7	1.500(2)	1.5145	1.5008	1.5039	1.5065	1.5030	1.4994	1.4989
C2–C3	1.427(2)	1.4053	1.4382	1.4386	1.4366	1.4322	1.4271	1.4247
C6–C5	1.394(3)	1.3972	1.4118	1.4103	1.4099	1.4036	1.3997	1.3954
C5–C4	1.384(3)	1.3984	1.4080	1.4050	1.4129	1.4067	1.4041	1.3933
C3–C4	1.373(3)	1.3874	1.3758	1.3758	1.3764	1.3700	1.3855	1.3833
C9–C10	1.512(2)	1.5294	1.5251	1.5278	1.5271	1.5227	1.5190	1.5175
C10–C11	1.521(2)	1.5328	1.5333	1.5335	1.5334	1.5295	1.5261	1.5286
Sq MSD ^c		0.021	0.016	0.015	0.016	0.014	0.009	0.007
A ^d	409	108	697	692	753	794	389	413

^aBond lengths are in Å. ^bVariants of calculations: A - monomer at B3LYP/6-31+G(d,p) level, gas phase in vacuum; B - molecule (I) of the optimized tetramer, B3LYP/6-31+G(d,p), PCM in water; C - molecule (II) of the optimized tetramer, B3LYP/6-31+G(d,p), PCM in water; D - optimized monomer, B3LYP/6-31+G(d,p), PCM in water; E - monomer, optimized at B3LYP/6-31++G(2d,2p) level, PCM in water; F - monomer, optimized at MP2/6-31+G(d,p) level, PCM in water; G - monomer, optimized at MP2/6-31++G(2d,2p), PCM in water. ^cSquare roots of mean squared deviations of calculated from experimental distances. ^dA - variance of bond lengths (in Å² × 10⁶ in a phenyl ring, equal to 1/6Σ(r_i - r_{avg})² × 10⁶, cf.,²⁶ r_i is a particular bond length, and r_{avg} is an average ring bonds length in a given experiment or calculation.

Table 2. Intermolecular Hydrogen Bonds in 1 and 2

compound 1	D–H...A (Å)	D–H (Å)	H...A (Å)	D...A (Å)	∠(D–H...A) (deg)
measured	N8–H81...O1 ⁱ	0.86(2)	1.87(2)	2.708(2)	165(2)
measured	N8–H82...O1 ⁱⁱ	0.86(2)	1.88(2)	2.733(2)	171(2)
calculated ^a	N8–H81...O1 ⁱ	1.057	1.757	2.782	169.0
calculated ^a	N8–H82...O1 ⁱⁱ	1.051	1.776	2.805	165.1
compound 2					
measured	N8–H81...O1 ⁱ	0.93(3)	1.80(3)	2.721(2)	171(2)
measured	N8–H82...O1 ⁱⁱ	0.88(2)	1.92(2)	2.765(2)	161(2)
calculated ^a	N8–H81...O1 ⁱ	1.045	1.819	2.847	167.3
calculated ^a	N8–H82...O1 ⁱⁱ	1.043	1.905	2.923	164.5

^aTetramer. B3LYP/6-31+G(d,p). PCM in water. ε = 78.4 Symmetry codes: (i) x, 1 + y, z; (ii) -x, 1 - y, 1 - z. for (1) and (i) 1 - x, 1 - y, 1 - z; (ii) 1 + xyz for (2).

(see further) — it is in agreement with the theory predicting stronger vibronic coupling in hydrogen bonds, when there is electronic coupling in excited vibronic levels.

Nevertheless, only calculations of tetramers provide proper descriptions of the pattern of intermolecular hydrogen bonds established in the crystals. Table 2 presents the comparison of

the results of calculations for tetramers at the B3LYP/6-31+G(d,p) level in water with related experimental values.

In both cases, the calculated hydrogen bonds are nearly linear. The experiment reveals shorter/stronger hydrogen bonds in **1** than in **2** despite higher acidity of the phenol in **2**. It seems natural, because in polar hydrogen bonds, the higher proton affinity of *p*-bromophenolate anion leads to stronger interaction with the acidic part of a complex. Calculations properly reproduce this feature of hydrogen bonds, yet for both molecules give longer hydrogen bonds than the experimental ones.

Because of a low reliability of the hydrogen position determination in X-ray crystallography experiments, we were able to efficiently compare only the distances between heavy atoms.

The discrepancy between experiment and calculations can result from higher permittivity of surroundings applied in calculations, in comparison with real values in the crystal. For this reason, we have undertaken wide studies on the influence of surrounding polarity on the calculated length of hydrogen bonds using the PCM model. The B3LYP/6-31+G(d,p) was applied to carry out the time-consuming calculations of tetramers. The results for solvents with electric relative permittivity within the range of 3–38 are presented in Table 3.

The first of investigated solvents has the permittivity seriously decreased in relation to water. At these conditions, the pattern of hydrogen bonds in two cycles like in the solid is properly reproduced. The O...N distances are lower than in water (cf. Table 2), which is in agreement with the interpretation given above, that too high permittivity of water led to extension of the length of zwitterionic hydrogen bond. The hydrogen bonds are still longer than in the solid state.

In the next solvents starting from methanol the external hydrogen bonds, in relation to forming the $R_4^2(8)$ cycle, became the molecular ones. This structure is presented in Supporting Information as Figure S3. The internal $R_4^2(8)$ ring is still persisting. The experimental value for powdered crystals measured according to a previously described procedure,²⁵ gave a value of relative permittivity equal to $3.1 \pm 2\%$. The last three solvents (Table 3) have similar permittivities. Nevertheless, the further decrease of the hydrogen bond length was not sufficient to obtain the experimental one. Similar results have been obtained for the gas phase. It demonstrates that the natural tendency for Mannich base with *para*-Br substituent is to be the molecular one, and the factor keeping the ionic type of hydrogen bond is the formation of tetramer. Nevertheless, the surrounding of such cycle is different than in the crystal structure, and calculated hydrogen bond lengths are not equal to experimental ones.

For compound **2** the calculations in acetonitrile give a decrease of NH...O distances, but they are still too long, because the electric permittivity of surroundings was too high. However, the calculations with the next solvents of decreasing electric permittivity result in serious modification of the pattern of hydrogen bonds (cf. Figure S4 in Supporting Information). The $R_4^2(8)$ ring appears to be broken and the $R_4^4(24)$ ring becomes more flexible, which leads to more linear and stronger NH...O hydrogen bonds. The N...O distance becomes even shorter than in experiment.

Summarizing the results of calculations one can state that formation of a specific tetrameric structure is a prerequisite for the formation of the O...H–N⁺ hydrogen bonds. The enhanced electric permittivity is the next necessary condition. Because the experimental value of relative permittivity is only

Table 3. Intermolecular Hydrogen Bonds in **1** and **2**, Results of B3LYP/6-31+G(d,p), PCM Calculations

Compound 1					
solvent (ϵ)	D–H...A (Å)	D–H (Å)	H...A (Å)	D...A (Å)	$\angle(D-H...A)$ (deg)
acetonitrile (35.7)	N8–H81...O1 ⁱ	1.058	1.719	2.761	167.1
	N8–H82...O1 ⁱⁱ	1.064	1.703	2.753	168.5
methanol (32.6)	^a N8–H81...O1 ⁱ	1.056	1.739	2.775	165.8
	^a N8–H82...O1 ⁱⁱ	1.063	1.706	2.758	169.5
ethanol (24.9)	^a N8–H81...O1 ⁱ	1.056	1.738	2.774	165.9
	^a N8–H82...O1 ⁱⁱ	1.063	1.706	2.758	169.5
chloroform (4.71)	^a N8–H81...O1 ⁱ	1.058	1.719	2.760	167.1
	^a N8–H82...O1 ⁱⁱ	1.064	1.702	2.752	168.5
diethylamine (3.58)	^a N8–H81...O1 ⁱ	1.059	1.700	2.751	168.3
	^a N8–H82...O1 ⁱⁱ	1.064	1.712	2.755	168.2
dibutyl ether (3.05)	^a N8–H81...O1 ⁱ	1.060	1.709	2.753	167.4
	^a N8–H82...O1 ⁱⁱ	1.064	1.699	2.749	167.1
das phase (1.00)	^a N8–H81...O1 ⁱ	1.067	1.683	2.734	167.2
	^a N8–H82...O1 ⁱⁱ	1.064	1.678	2.729	168.7
Compound 2					
solvent (ϵ)	D–H...A (Å)	D–H (Å)	H...A (Å)	D...A (Å)	$\angle(D-H...A)$ (deg)
acetonitrile (35.7)	N8–H81...O1 ⁱ	1.046	1.808	2.838	167.6
	N8–H82...O1 ⁱⁱ	1.042	1.921	2.931	162.3
methanol (32.6)	R(24) ring structure	1.066	1.649	2.710	172.8
			1.061	1.671	2.719
ethanol (24.9)	R(24) ring structure	1.066	1.650	2.711	172.9
			1.061	1.667	2.715
chloroform (4.71)	R(24) ring structure	1.067	1.635	2.685	167.1
			1.076	1.593	2.664
diethylamine (3.58)	R(24) ring structure	1.068	1.627	2.681	167.9
			1.078	1.587	2.660
dibutyl ether (3.05)	R(24) ring structure	1.070	1.614	2.668	167.3
			1.080	1.583	2.657
gas phase (1.00)	R(24) ring structure	1.106	1.485	2.585	172.7
			1.085	1.549	2.615

^aStructures with the molecular form of other hydrogen bonds in the R(12) ring.

$3.1 \pm 2\%$ for both compounds, the lowest polar solvents (diethyl amine and dibutyl ether) applied here should be the best models in our calculations.

In **1** at this permittivity the tetrameric pattern of ionic hydrogen bonds in the $R_4^2(8)$ cycle is reproduced, and the O...N distances are shorter than in water, but still longer than in the solid state. Additional interactions in all the systems of hydrogen bonds are probably the reason for incomplete reproduction of the experiment by calculation. One can mention that at this permittivity, the “external” hydrogen bonds in relation to the $R_4^2(8)$ ring become molecular ones. These “peripheric” hydrogen bonds, not involved in tetramers, reveal properties characteristic for weak hydrogen bonds, in **1**. Simultaneously, the surroundings of central tetramers becomes different than in the solid state. In **2** only water and acetonitrile allow keeping the pattern of hydrogen bonds like in the solid state, and too high permittivity leads to extension of the ionic hydrogen bonds. Calculations with other solvents with

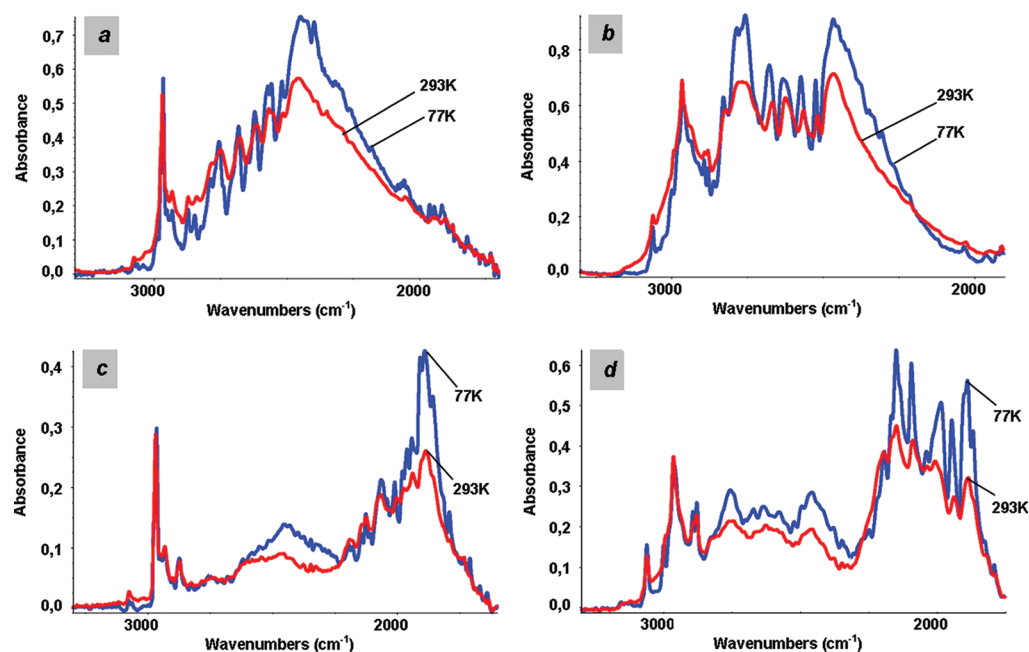


Figure 7. IR spectra of polycrystalline samples of **1** and **2** measured in KBr pellets at 293 and 77 K in the frequency range of the $\nu_{\text{N-H}}/\nu_{\text{N-D}}$ bands. a – compound **1**, b – compound **2**, c – spectra of isotopically diluted **1** (80% D, 20% H), d – spectra of isotopically diluted **2** (70% D, 30% H).

decreasing electric permittivity result in serious modification of the pattern of hydrogen bonds. The R_4^2 (8) ring is broken and a more flexible $R_4^4(24)$ ring leads to more linear and stronger $\text{NH}^+\cdots\text{O}^-$ hydrogen bonds. The $\text{N}\cdots\text{O}$ distance becomes even shorter than in experiment, however, for other hydrogen bond patterns than in experiments.

IR Spectra of KBr Pellets. The IR spectra of polycrystalline samples of **1** measured in the $\nu_{\text{N-H}}$ band frequency range of the proton stretching vibration band by the KBr pellet method at 293 and 77 K are shown in Figure 7a. The band exhibits a two-branch fine structure pattern, which is not homogeneous. The lower-frequency branch intensity ($2500\text{ cm}^{-1} - 2100\text{ cm}^{-1}$) grows when temperature decreases. The intensity of the higher-frequency branch of the band ($2900\text{ cm}^{-1} - 2500\text{ cm}^{-1}$) remains practically stable in these circumstances.

The corresponding IR spectrum of **2** measured in the analogous circumstances is given in Figure 7b. The $\nu_{\text{N-H}}$ band also exhibits a two-branch structure. The two spectral branches of the band ($2600\text{ cm}^{-1} - 2200\text{ cm}^{-1}$) and ($2850\text{ cm}^{-1} - 2600\text{ cm}^{-1}$) are susceptible to the influence of temperature as in the case of **1**.

Isotopic Dilution Effects in the Spectra. The IR spectrum of polycrystalline samples of isotopically diluted **1** (ca. 80% D and 20% H) measured at two different temperatures in the frequency range of the “residual” $\nu_{\text{N-H}}$ band is shown in Figure 7c. The “residual” $\nu_{\text{N-H}}$ band when compared with the corresponding spectrum of the isotopically neat substance lost its own characteristic two-band fine structure pattern.

On the other hand, the $\nu_{\text{N-D}}$ band, in spite of its different shape, in some aspects qualitatively resembles the $\nu_{\text{N-H}}$ band shape (the band is ca. 1.5 times narrower). This H/D isotopic effect is familiar in the IR spectroscopy of the hydrogen bond formed in diverse molecular systems.^{29,30}

The corresponding spectra of isotopically diluted polycrystalline samples of **2** (ca. 70% D) measured in the frequency range of the “residual” $\nu_{\text{N-H}}$ band and the $\nu_{\text{N-D}}$ band, at two different

temperatures, are shown in Figure 7d. The “residual” $\nu_{\text{N-H}}$ band contour retained its characteristic two-branch structure when compared with the band properties of the isotopically neat substance. The branch ranges are $2200\text{ cm}^{-1} - 1950\text{ cm}^{-1}$ and $1950\text{ cm}^{-1} - 1800\text{ cm}^{-1}$. It means that isotopic dilution exerted no influence on the interhydrogen bond couplings in the tetramers of **2**. Therefore, no changes in the band characteristics resulted from the isotopic dilution.

Polarized IR Spectra of Crystals of 1. The polarized IR spectra of **1** single crystals measured at 77 K in the frequency range of the $\nu_{\text{N-H}}$ band are shown in Figure 8a. They proved that the dichroic properties in the band range are constant in the whole band range, which is a typical property of hydrogen bond tetramers with four mutually coupled moieties. An analysis of the polarized IR spectra of **2** was not possible since the substance did not crystallize from melt, forming glass samples instead.

The Isotopic Dilution Effects in the $\nu_{\text{N-H}}$ and $\nu_{\text{N-D}}$ Bands. Polarized IR spectra of isotopically diluted **1** single crystals (ca. 95% D and 5% H) measured at 77 K in the frequency range of the “residual” $\nu_{\text{N-H}}$ band and the $\nu_{\text{N-D}}$ band are shown in Figure 8b.

The two-branch structure of the $\nu_{\text{N-H}}$ and $\nu_{\text{N-D}}$ bands from the IR spectra of isotopically neat crystals results from vibrational exciton interactions involving hydrogen or deuterium bonds in the cyclic tetramers of the hydrogen or deuterium bonds in the crystals. In these exciton couplings, the adjacent hydrogen bonds in the tetramers take place. It means that interactions of a “head-to-tail” type occur via electrons of the systems in the R(8)-type chain. This kind of exciton interactions differs essentially from the “through-space” or the “side-to-side” type interactions involving hydrogen bonds. Such interactions could exist in the R(12) chain, cf. Figure 5, but the distance between two parallel hydrogen bonds is 3.541 and 3.553 Å, and it is probably too high for the “side-to-side” interactions.

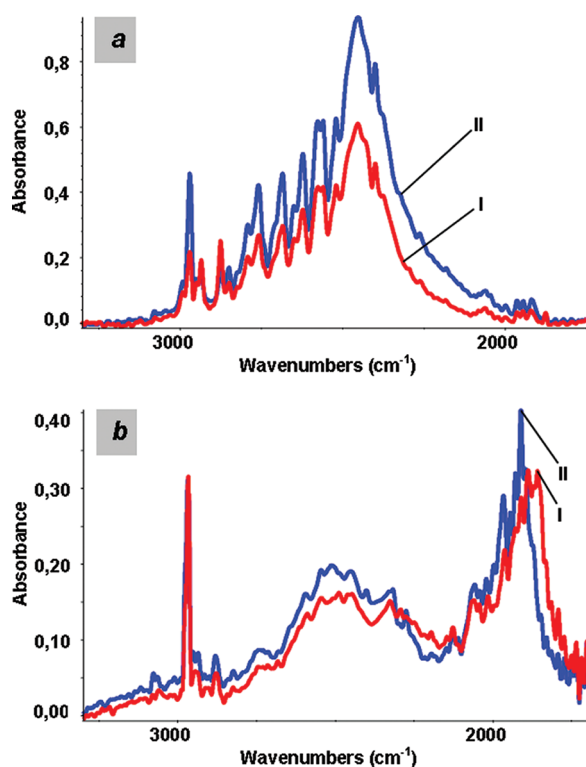


Figure 8. Polarized IR spectra of **1** single crystal measured at 77 K in the frequency range of the $\nu_{\text{N-H}}/\nu_{\text{N-D}}$ bands. I: E || a; II: E || b. (a) H-1. (b) D-1.

For the isotopically diluted crystals (less than 20% H), on assuming a fully random distribution of protons and deuterons in the hydrogen bridge systems, the probability of the closest adjacency of protons in the tetramers is very low. In these circumstances, the spectral effects of the exciton couplings in the crystalline spectra should disappear.²² However, the recent studies of isotopically diluted hydrogen-bonded crystals have proved that in the case of cyclic hydrogen bond aggregates (dimers,^{19,20} trimers,²¹ and tetramers²) the distribution of protons and deuterons is not random. These effects result from the so-called “dynamical co-operative interactions” in hydrogen bond systems,²⁰ which originate from Herzberg–Teller-type vibronic couplings,²⁰ involving the proton stretching vibrations and electronic motions in the systems. The “dynamical co-operative interactions” are responsible for an “attraction” of identical hydrogen isotope atoms in systems of mutually coupled hydrogen bonds in isotopically diluted crystals. Therefore, the vibrational exciton interactions involving the adjacent hydrogen bonds in the lattice are retained even in the case of samples with low concentrations of protons. This allows for the invariability of the “residual” $\nu_{\text{N-H}}$ band shapes, regardless of the growing isotopic exchange rates in the samples. It is possible when the “dynamical co-operative interaction” energy is approximately equal to 1.5 kcal/mol of hydrogen bond dimers.¹⁹

The “residual” $\nu_{\text{N-H}}$ band contour in the spectra of isotopically diluted **1** differs by shape from the corresponding band characteristics for isotopically neat samples. This is most probably due to a fairly random distribution of protons and deuterons in the case of hydrogen-bonded crystals.²² Recent studies have proved that such property is relatively rare in nature. In the case of crystals of **1** it results from a relatively

weak vibronic coupling in the tetramers and from weak “dynamical co-operative interactions” involving the hydrogen bonds. In these circumstances the vibrational exciton interactions in the cyclic tetramers vanish. In consequence, the $\nu_{\text{N-H}}$ band contour evolution along with the growing concentration of deuterons in the sample depends on the disappearance of its two-branch structure.

The $\nu_{\text{N-H}}$ and $\nu_{\text{N-D}}$ bands in the spectra of isotopically neat **2** samples exhibit two-branch fine structures resulting from the exciton couplings between the hydrogen or deuterium bonds in cyclic tetramers of the compound. Similarly as in hydrogen bond chains, the couplings involve the adjacent closely spaced hydrogen or deuterium bonds in the cyclic structures, leading to an identical two-branch structure of the $\nu_{\text{N-H}}$ or $\nu_{\text{N-D}}$ bands. These exciton interactions of the “head-to-tail” type, occurring via electrons, are effective for the coupled moieties containing identical hydrogen isotopes - protons or deuterons. On assuming a “through-space” coupling in the tetramers the deduced band contours are different.²¹

The “residual” $\nu_{\text{N-H}}$ band in the IR spectra of isotopically diluted **2** samples (of high concentration of deuterons) is almost identical with the $\nu_{\text{N-H}}$ band contour of the neat substance. This effect results from the fully nonrandom distribution of the hydrogen isotopes in the cyclic tetramers.¹⁸

It means that in spite of the very low concentration of the “residual” protons in the samples, the hydrogen bond tetramers contain identical hydrogen isotope atoms in the entire cycles. This fact results from a relatively strong vibronic coupling in the tetramers of **2**, correlating with strong “dynamical co-operative interactions” involving hydrogen bonds in the tetramers, which energetically favors the tetramers with identical hydrogen isotopes in a cycle (the H/D isotopic “self-organization” effects). This allows for retaining of the full system of exciton interactions in tetramers, which in turn is responsible for the invariance of the “residual” $\nu_{\text{N-H}}$ band contour along with the increasing concentration of deuterons.¹⁹

The Role of the Substituent Groups. Measurements of the IR spectra of polycrystalline samples of the two compounds have proved that the substituent atomic groups, Br and NO₂, influenced the IR spectral properties of hydrogen bonds in the cyclic tetramers. This effect is a result of a differentiation of subtle changes in the electronic properties of the atomic cores in the cycles exerted by these substituent groups in the two individual crystalline systems. The analysis of the spectra shows that the Br and NO₂ substituents in a different way influence the magnitude of “dynamical co-operative interaction” energies in the two individual types of the hydrogen bond tetramers. As a consequence, the two individual systems differ from each other by the way in which the H/D isotopic “self-organization” processes occur in the isotopically diluted crystals. For **1** crystals the “dynamical co-operative interaction” energies are much lower than 3 kcal/mol of the tetramers. This energy value does not guarantee holding together identical hydrogen isotope atoms in the tetramers of the compound in isotopically diluted crystals.^{19,20}

For **2** crystals the energy of the “dynamical co-operative interactions” is at least equal to 3 kcal/mol of the tetramers.^{17,18} This is sufficient for the invariance of the “residual” $\nu_{\text{N-H}}$ band contour shape, in spite of the growing concentration of deuterons in the crystals.

CONCLUSIONS

Two secondary Mannich bases revealing zwitterionic structures in the solid state were synthesized. They are derivatives of *n*-propylamine and *p*-bromophenol (**1**) or *p*-nitrophenol (**2**). Analogous structures of tertiary Mannich bases can also form the ionic forms but in the case of *p*-Br derivatives, the ionic structures generally are not formed due to weak acidity of phenol. It was shown that the formation of tetramer structure in the crystal makes it possible to obtain the zwitterionic forms also in **1**. Some enhanced electric permittivity is also the required condition. B3LYP/6-31+G(d,p) PCM calculations support such an interpretation. Water was used as a solvent in the first calculations. It appeared however that too long hydrogen bonds were obtained because the known effect of weakening of the ionic hydrogen bonds in polar solvents. Acetonitrile with twice lower permittivity gave shorter hydrogen bridges but still longer than in experiment. Experimentally determined permittivity of both crystal was $3 \pm 2\%$. It was stated however that further decrease of permittivity in calculations leads to substantial change of the pattern of hydrogen bonds and because of that the calculated structures are different than in experiment. Different behavior of molecules with *p*-Br and *p*-NO₂ substituents was found. Probably more extended systems should be calculated, taking into account interactions with further surrounding molecules. It appeared too complicated to take into account more molecules in calculations than in tetramer, at present.

The unique technique for obtaining the monocrystalline probes from the melt allowed measuring the IR spectra in polarized light. An IR study of almost completely deuterated (N-D) species was applied to inspect the interaction between hydrogen bonds in the crystal. Spectral features, appearance of the allowed and nonallowed ν_{N-H} vibrations in the -NH₂ moiety, demonstrate a coupling between hydrogen bonds in neat hydrogen species in both compounds. The "residual" N-H species in deuterated probes show that only in the *p*-NO₂ derivative (**2**) isotopic self-organization takes place. It demonstrates the stronger interactions in the crystal of **2**. On the other hand, the geometric considerations prove the existence of stronger hydrogen bonds in **1**. On the basis of quantum mechanical calculations and inspection of crystal structure, the stronger electronic coupling in molecule **2** was stated. It explains stronger interaction between hydrogen bonds in crystal of **2**, according to the theory that specific organization of isotopes (H and D) in isotopically heterogeneous species is possible only with participation of electronic interactions in excited vibronic levels. The effects demonstrated here do not result from the acid-base interactions balance in the hydrogen bond as the hydrogen bond in **2** is weaker than in **1**.

ASSOCIATED CONTENT

Supporting Information

Extended tables related to the crystallographic structure determination, lists of weak intermolecular contacts, figures depicting crystal packing of **1** and **2**, and crystal structure reports in the CIF format for **1** and **2**. Table of energy values and calculated dipole moments for compounds **1** and **2**. This material is available free of charge via the Internet at <http://pubs.acs.org>.

AUTHOR INFORMATION

Corresponding Author

*E-mail: akoll@chem.uni.wroc.pl (A.K.); jerzyk@elrond.chem.uni.wroc.pl (J.K.); telephone: +48-71-3757200; fax: +48-71-3282348 (J.K.).

ACKNOWLEDGMENTS

The authors gratefully acknowledge the Wrocław Centre for Networking and Supercomputing (WCSS) for providing computer time and facilities. A.A.-W. and A.S. acknowledge the financial support of Warsaw University of Technology. J.K. and A.K. are very thankful to Dr. Jarosław Panek for kindness and fruitful discussion, and to Professor Hubert Kołodziej and Dr. Magdalena Kosmowska for performing of dielectric permittivity measurements.

REFERENCES

- (1) Koll, A.; Wolschann, P. *Monatsh. Chem.* **1996**, *127*, 477–486.
- (2) Koll, A.; Wolschann, P. *Monatsh. Chem.* **1999**, *130*, 983–1001.
- (3) Rutkowski, K.; Koll, A. *J. Mol. Struct.* **1994**, *322*, 195–203.
- (4) Schreiber, V.; Koll, A.; Sobczyk, L. *Bull. Acad. Pol. Sci. Ser. Sci. Chim.* **1978**, *26*, 651–654.
- (5) Rospenk, M.; Koll, A. *Pol. J. Chem.* **1993**, *67*, 1851–1858.
- (6) Słowikowska, J.; Beagley, B.; R. G. Pitchard, R. G.; Wozniak, K. *J. Mol. Struct.* **1994**, *317*, 99–110.
- (7) Jezierska, A.; Panek, J.; Filarowski, A. *J. Chem. Inf. Model.* **2007**, *47*, 818–831.
- (8) Jezierska, A.; Panek, J.; Koll, A.; Mavri, J. *J. Chem. Phys.* **2007**, *126*, 205101.
- (9) Jezierska, A.; Panek, J.; Borštnik, U.; Mavri, J.; Janežič, D. *J. Phys. Chem. B.* **2007**, *111*, 5243–5248.
- (10) Jezierska, A.; Panek, J. *J. Chem. Theor. Comput.* **2008**, *4*, 375–384.
- (11) Bujnowski, K.; Adamczyk, A.; Synoradzki, L. *Org. Prep. Proced. Int.* **2007**, *39*, 153–184.
- (12) Bujnowski, K.; Adamczyk-Woźniak, A.; Synoradzki, L. *Arhivov. 2008*, *13*, 106–114.
- (13) Kołodziejczak, J.; Adamczyk-Woźniak, A.; Sporzyński, A.; Kochel, A.; Koll, A. *J. Mol. Struct.* **2010**, *976*, 290–296.
- (14) Majerz, I.; Głowiak, T.; Koll, T. *J. Mol. Struct.* **1996**, *374*, 339–345.
- (15) Etter, M. C. *Acc. Chem. Res.* **1990**, *23*, 120–126.
- (16) Etter, M. C.; MacDonald, J. C.; Bernstein, J. *Acta Crystallogr. B* **1990**, *46*, 256–262.
- (17) Koll, A.; Głowiak, T. *J. Cryst. Spectr. Res.* **1985**, *15*, 411–421.
- (18) (a) Flakus, H. T.; Miros, A. *J. Mol. Struct.* **1999**, *484*, 103–115. (b) Flakus, H. T.; Miros, A. *Spectrochim. Acta A* **2001**, *57*, 2391–2401. (c) Flakus, H. T.; Tyl, A.; Jones, P. G. *Spectrochim. Acta A* **2002**, *58*, 299–310. (d) Flakus, H. T.; Miros, A. *Spectrochim. Acta A* **2002**, *58*, 225–237. (e) Flakus, H. T.; Chelmecki, M. *Spectrochim. Acta A* **2002**, *58*, 179–196. (f) Flakus, H. T.; Machelska, A. *Spectrochim. Acta A* **2002**, *58*, 555–568. (g) Flakus, H. T.; Miros, A.; Jones, P. G. *J. Mol. Struct.* **2002**, *604*, 29–44. (h) Flakus, H. T.; Chelmecki, M. *Spectrochim. Acta A* **2002**, *58*, 1867–1880. (i) Flakus, H. T. *Pol. J. Chem.* **2003**, *77*, 489–517. (j) Flakus, H. T.; Chelmecki, M. *J. Mol. Struct.* **2003**, *659*, 103–117. (k) Flakus, H. T.; Tyl, A.; Jones, P. G. *Vibr. Spectr.* **2003**, *33*, 163–175. (l) Flakus, H. T.; Michta, A. *Vibr. Spectr.* **2003**, *33*, 177–187. (m) Flakus, H. T.; Chelmecki, M. *J. Mol. Struct.* **2004**, *705*, 81–89. (n) Flakus, H. T.; Michta, A. *J. Mol. Struct.* **2004**, *707*, 17–31. (o) Flakus, H. T.; Jabłońska, M. *J. Mol. Struct.* **2004**, *707*, 7–108. (p) Flakus, H. T.; Michta, A. *J. Mol. Struct.* **2005**, *741*, 19–29. (q) Benmalti, M. E.; Blaise, P.; Flakus, H. T.; Henri-Rousseau, O. *Chem. Phys.* **2006**, *320*, 267–274. (r) Flakus, H. T.; Pyzik, A. *Chem. Phys.* **2006**, *323*, 479–489. (s) Flakus, H. T.; Jabłońska, M.; Jones, P. G. *Spectrochim. Acta A* **2006**, *65*, 481–489. (t) Flakus, H. T.; Stachowska, B. *Chem. Phys.* **2006**, *330*, 231–244. (u) Flakus, H. T.; Pyzik, A.; Michta, A.; Kusz, J. *Vibr. Spectr.* **2007**, *44*, 108–120.

- (v) Flakus, H. T.; Śmiszek-Lindert, W.; Stadnicka, K. *Chem. Phys.* **2007**, *335*, 221–232. (w) Flakus, H. T.; Tyl, A. *Chem. Phys.* **2007**, *336*, 36–50. (x) Flakus, H. T.; Pyzik, A. *Chem. Phys. Res. J.* **2007**, *1*, 49–60. (y) Flakus, H. T.; Hachuła, B. *Chem. Phys.* **2008**, *345*, 49–64. (z) Flakus, H. T.; Tyl, A. *Vibr. Spectr.* **2008**, *47*, 129–138. (aa) Flakus, H. T.; Jabłońska, M.; Kusz, J. *Vibr. Spectr.* **2009**, *49*, 174–182. (ab) Flakus, H. T.; Michta, A. *Vibr. Spectr.* **2009**, *49*, 142–154. (ac) Marczak, W.; Kielek, K.; Czech, B.; Flakus, H. T.; Rogalski, M. *Phys. Chem. Chem. Phys. (PCCP)* **2009**, *11*, 2668–2678. (ad) Flakus, H. T.; Jabłońska, M.; Tyl, A. *Pol. J. Chem.* **2009**, *83*, 869–886. (ae) Flakus, H. T.; Tyl, A.; Jabłońska, M. *Chem. Phys.* **2009**, *364*, 76–89. (af) Rekik, N.; Ghalla, H.; Flakus, H. T.; Jabłońska, M.; Blaise, P.; Oujia, B. *Chem. Phys. Chem.* **2009**, *10*, 3021–3033. (ag) Rekik, N.; Ghalla, H.; Flakus, H. T.; Jabłońska, M.; Oujia, B. *J. Comput. Chem.* **2010**, *31*, 463–475. (ah) Rekik, N.; Ghalla, H.; Michta, A.; Oujia, B.; Flakus, H. T. *Spectrochim. Acta A* **2010**, *75*, 37–47. (ai) Flakus, H. T.; Michta, A. *J. Phys. Chem. A* **2010**, *114*, 1688–1698. (aj) Flakus, H. T.; Hachuła, B. *Chem. Phys.* **2010**, *368*, 133–145. (ak) Flakus, H. T.; Hachuła, B.; Pyzik, A. *Chem. Phys.* **2011**, *379*, 73–82. (al) Flakus, H. T.; Tyl, A.; Maślankiewicz, A. *J. Phys. Chem. A* **2011**, *115*, 1027–1039. (am) Flakus, H. T.; Hachuła, B. *Vibr. Spectr.* **2011**, *56*, 170–176. (an) Flakus, H. T.; Michta, A.; Nowak, M.; Kusz, J. *J. Phys. Chem. A* **2011**, *115*, 4202–4213.
- (19) Flakus, H. T.; Bańczyk, A. *J. Mol. Struct.* **1999**, *476*, 57–68.
- (20) Flakus, H. T. *J. Mol. Struct.* **2003**, *646*, 15–23.
- (21) Flakus, H. T.; Pyzik, A. *Chem. Phys.* **2006**, *323*, 479–489.
- (22) Flakus, H. T.; Pyzik, A. *Vibr. Spectr.* **2006**, *41*, 28–36.
- (23) Sheldrick, G. M. *Acta Crystallogr. A* **2008**, *64*, 112–122.
- (24) Frisch, M. J.; Trucks, G. W.; Schlegel, H. B.; Scuseria, G. E.; Robb, M. A.; Cheeseman, J. R.; Scalmani, G.; Barone, V.; Mennucci, B.; Petersson, G. A.; Nakatsuji, H.; Caricato, M.; Li, X.; Hratchian, H. P.; Izmaylov, A. F.; Bloino, J.; Zheng, G.; Sonnenberg, J. L.; Hada, M.; Ehara, M.; Toyota, K.; Fukuda, R.; Hasegawa, J.; Ishida, M.; Nakajima, T.; Honda, Y.; Kitao, O.; Nakai, H.; Vreven, T.; Montgomery, J. A., Jr.; Peralta, J. E.; Ogliaro, F.; Bearpark, M.; Heyd, J. J.; Brothers, E.; Kudin, K. N.; Staroverov, V. N.; Kobayashi, R.; Normand, J.; Raghavachari, K.; Rendell, A.; Burant, J. C.; Iyengar, S. S.; Tomasi, J.; Cossi, M.; Rega, N.; Millam, N. J.; Klene, M.; Knox, J. E.; Cross, J. B.; Bakken, V.; Adamo, C.; Jaramillo, J.; Gomperts, R.; Stratmann, R. E.; Yazyev, O.; Austin, A. J.; Cammi, R.; Pomelli, C.; Ochterski, J. W.; Martin, R. L.; Morokuma, K.; Zakrzewski, V. G.; Voth, G. A.; Salvador, P.; Dannenberg, J. J.; Dapprich, S.; Daniels, A. D.; Farkas, Ö.; Foresman, J. B.; Ortiz, J. V.; Cioslowski, J.; Fox, D. J. *Gaussian 09*, Revision A.02; Gaussian, Inc.: Wallingford, CT, 2009.
- (25) Szulia, S.; Kolodziej, H. A.; Szuszkiewicz, W.; Czupińska, W. G. *J. Non-Cryst. Solids* **2010**, *356*, 805–808.
- (26) Koll, A.; Melikova, S. M.; Karpfen, A.; Wolschann, P. *J. Mol. Struct.* **2001**, *559*, 127–145.
- (27) Linde, D. R. *CRC Handbook of Chemistry and Physics*, 85th ed.; CRC Press: Boca Raton, 2004–2005; Chapter 8, pp 8–50.
- (28) Schuster, P.; Zundel, G.; Sandorfy, C. *The Hydrogen Bond*; North-Holland: Amsterdam, 1976.
- (29) Marechal, Y. *The Hydrogen Bond and The Water Molecule: The Physics and Chemistry of Water, Aqueous and Bio-Media*; Elsevier, Amsterdam, 2006.
- (30) Mikhailov, I. D.; Savelev, V. A.; Sokolov, N. D.; Bokh, N. G. *Phys. Status Solidi* **1973**, *57*, 719–732.